Atom Indonesia

Journal homepage: https://atomindonesia.brin.go.id

Proton and Helium-4 Ion Beams for Hadron Therapy: Depth, Lateral, and Secondary Particle Dose Calculations

O. Allaoui[1], A. Didi[2*], E. M. Alibrahmi[1], E. M. Chakir[1], Z. Sadoune[3]

[1]*Laboratory of Materials Physics and Subatomics Laboratory, Physics Department, University Ibn Tofail, Kenitra, Morocco*
[2]*Laboratory of Sciences and Health Technologies, High Institute of Health Sciences, Hassan First University of Settat, BP 555, Settat, 26000, Morocco*
[3]*Laboratory of Electronic Systems, Information Processing, Mechanics, and Energy, Physics Department, University Ibn Tofail, Kenitra, Morocco*

ARTICLE INFO

Article history:
Received 1 June 2025
Received in revised form 3 August 2025
Accepted 4 August 2025

Keywords:
Monte carlo simulation
Hadrotherapy
Proton beam
Helium-4 beam
Dose distribution

ABSTRACT

This study compares Monte Carlo simulations of dose distributions from proton and helium-4 ion beams in an aqueous medium using the MCNP code. Proton beams (60-240 MeV) and helium-4 beams (80-240 MeV, 520 MeV) are evaluated for their ballistic properties in hadron therapy, including penetration depth, lateral dose spread, and secondary particle production. Helium-4 ions, with higher mass and charge, exhibit sharper Bragg peaks and less lateral scattering than protons, suggesting better dose conformity. They also produce fewer long-range secondary particles, potentially reducing unintended dose to healthy tissues. These results highlight the potential of helium-4 ions as a viable alternative to proton therapy for more precise dose control and reduced collateral damage.

© 2026 Atom Indonesia.
Published by BRIN Publishing. AI is ESCI and Scopus indexed. This is an open access article CC BY-NC-SA license (https://creativecommons.org/licenses/by-nc-sa/4.0/).

INTRODUCTION

Hadron therapy offers significant advantages over conventional photon treatments [1]. Unlike photons, hadrons (protons and heavy ions such as those of helium-4) deposit most of their energy in a highly localized region (the Bragg peak) [2-4], allowing for precise tumor targeting while preserving surrounding healthy tissues [5,6]. This unique property makes hadron therapy a preferred option for treating complex cancers, particularly pediatric tumors, radio-resistant neoplasms, or lesions near critical organs (such as the brain, spinal cord, or salivary glands) [7]. Currently, protons dominate clinical applications, but heavier ions (of carbon or helium-4) are gaining interest due to their higher Relative Biological Effectiveness (RBE) and reduced lateral scattering, making them particularly suitable for hypoxic tumors or those with a low control ratio [8-10]. However, their nuclear fragmentation and energy response require precise modeling to optimize therapeutic protocols [11].

In this study, we analyzed dose distributions induced by proton and helium-4 ion beams in an aqueous medium (water), simulated using Monte Carlo methods. Our simulations compared proton beams (60-240 MeV, in 20 MeV steps) and helium-4 ion beams (80-240 MeV, plus 520 MeV, in 40 MeV steps), evaluating their penetration, fragmentation, dose profiles, and secondary particles generation. In practice, these beam energies are produced using particle accelerators such as cyclotrons or synchrotrons. Proton and helium-4 ion beams are accelerated to specific energies by controlling the magnetic and electric fields within these machines. The selected energy ranges correspond to clinically relevant depths for therapeutic or research applications. Energy tuning is typically achieved by adjusting accelerator parameters or using energy selection systems that filter the beam before it reaches the target medium. The results obtained in this study help identify, among the particles studied (protons and ^{4}He ions), those offering the best

*Corresponding author.
E-mail address: abdessamad.didi1@usmba.ac.ma
DOI: https://doi.org/10.55981/aij.2026.1717

combination of ballistic precision and reduced peri-tumoral toxicity, compared to carbon ions [12]. This study aimed to assess the therapeutic potential of ^{4}He ions and protons for the treatment of superficial and ocular tumors. Although Monte Carlo N-Particle (MCNP) is a well-established and extensively validated simulation tool, the novelty of this work lies in its specific application to the modeling of therapeutic particle interactions in the context of ocular and superficial tumors, using adapted simulation geometries. No direct comparison with experimental data was made; however, the simulation results were discussed in relation to trends reported in the literature to highlight qualitative agreement [13,14]. These findings provide a foundation for future studies involving experimental validation and clinical optimization.

In addition to physical dose characteristics, the Relative Biological Effectiveness (RBE) of these beams plays a crucial role in clinical decision-making. Helium-4 ions exhibit a slightly higher RBE than protons, potentially leading to improved tumor control in hypoxic regions or radio-resistant tumors. While this study focused on physical interactions, a future extension including RBE modeling would further enhance the clinical relevance of the results.

METHOD AND MATERIAL

This study was conducted entirely using the Monte Carlo simulation code MCNP (version 6.3) [13]. The use of MCNP enabled detailed simulations of energy deposition and secondary particle transport [15]. For proton beams, eight clinically relevant energies were selected: 60, 80, 100, 120, 140, 160, 180, 200, and 220 MeV, covering the full range of therapeutic needs. These energies correspond to penetration depths required for treating tumors located at various anatomical sites, from shallow to deep-seated lesions, and are routinely used in clinical proton therapy to optimize dose delivery while sparing surrounding healthy tissue. For helium-4 ions, five standard energies (80, 120, 160, 200, and 240 MeV) were simulated, along with additional beams at 280, 320, 360, 400, 440, 480, and 520 MeV to examine the nuclear fragmentation phenomena [16]. These helium ion energies are clinically relevant because they enable precise dose localization with reduced lateral scattering compared to protons, and the extended energy range is essential for studying their potential application in treating deep-seated tumors and understanding their unique interaction characteristics, including fragmentation behavior. In MCNP, each beam was modeled as a perfectly collimated parallel source with a monoenergetic energy distribution and circular emission geometry of 50 mm in diameter, oriented along the Z-axis of the coordinate system. The 50 mm diameter was chosen to represent a clinically realistic field size commonly used in particle therapy for small to medium-sized tumors. This beam width provides a balance between computational efficiency and clinical relevance, ensuring adequate spatial resolution for dose distribution analysis while maintaining compatibility with typical treatment field dimensions.

Simulation geometry and dosimetric setup

This study employed the Monte Carlo simulation code MCNP version 6.3 to model the interactions of monoenergetic helium-4 (^{4}He) ion beams with a water-equivalent phantom. The ion beam was directed along the z-axis and modeled with a Gaussian spatial distribution, featuring a full width at half maximum (FWHM) of 1.5 cm in both the x and y directions. This setup mimics a clinically realistic beam profile and allows for accurate spatial characterization of lateral scattering and dose fall-off.

Water phantom

The simulation geometry included a cylindrical water phantom designed to replicate the dosimetric properties of human soft tissues. The cylinder measured 0.40 m in height and 0.20 m in diameter, with a density of 1000 kg/m^{3} (Table 1). Its longitudinal axis was aligned with the z-axis, matching the direction of beam propagation. This configuration ensured radial symmetry and minimized boundary effects.

The diameter was selected to fully contain the lateral spread of the beam, while the height was sufficient to accommodate the full range ofenergy deposition for both proton and helium-4 ion beams at therapeutic energies.

Dose scoring and analysis

The absorbed dose was scored throughout the water phantom for all radiation components, including primary helium-4 ions, secondary charged particles, neutrons, and gamma rays. Concentric cylindrical scoring regions were defined to evaluate both longitudinal (depth) and lateral dose distributions (as specified in Table 1).

Table 1. Geometric parameters of the monte carlo simulation (MCNP 6.3).

Component	Shape	Dimensions	Density (kg/m³)	Material	Main Function	Alignment
Water Phantom	Cylinder	Length: 0.40 m Diameter: 0.20 m	1000	Water-equivalent (H_2O)	Dose deposition medium Simulation of soft tissue equivalence	z-axis (beam)

Lateral dose profiles were extracted at approximately mid-range depth for each of the simulated beam energies to assess spatial resolution and scattering behavior. This approach provides a comprehensive dosimetric analysis essential for evaluating the clinical potential of helium ion therapy.

The atomic composition of each medium was specified in the MCNP material cards. The physical models activated in MCNP included ionization, Coulomb scattering, and both elastic and inelastic nuclear reactions [17], with modeling of light ions transport, detailed treatment of nuclear reactions at intermediate energies, the tracking of secondary particles and fragments resulting from nuclear fragmentation [18-21]. The dosimetric data were extracted with a spatial resolution of 10 mm × 10 mm × 10 mm. The cross-sections used were sourced from the ENDF/B-VIII.0 library. Thresholds were set at 1 keV for electrons and photons and 10^{-5} MeV for neutrons [22]. These values were chosen to account for energy deposition while maintaining optimal computational efficiency by avoiding tracking particles of low energy-deposition impact. To obtain statistically reliable results, each simulation was performed using 5×10^9 particle histories, ensuring a confidence level, with uncertainties below 1 % in the therapeutic regions of interest.

Validation of simulation results involved first a quantitative comparison with the reference data from ICRU [23]. Additionally, a systematic analysis of tally convergence was conducted to verify the numerical stability of the results [24]. Several independent simulations were performed to assess data reproducibility, and energy conservation checks were implemented to ensure the consistency of energy interactions throughout the simulation process [25].

RESULTS

Lateral dose distribution

Figure 1 presents the lateral dose distribution of proton beams at various energies. In this context, "lateral" refers to the direction perpendicular to the beam axis (i.e., the X and Y directions), while the beam itself propagates along the Z-axis. The figure demonstrates a strong dose depositionat lower energies, with a maximum value of 4.01 MeV/g observed at 80 MeV anda lateral radius of 0.5 mm. This elevated dose at low energy is due to the more intense interaction of protons with the medium over a shorter path, leading to higher energy deposition per unit volume. As the beam energy increased, the peak lateral dose decreased progressively, registering values of 3.29 MeV/g at 100 MeV, 2.89 MeV/g at 120 MeV, 2.53 MeV/g at 140 MeV, 2.22 MeV/g at 160 MeV, 2.01 MeV/g at 180 MeV, 1.86 MeV/g at 200 MeV, and 1.64 MeV/g at 240 MeV.

To improve clarity and focus on the clinically significant area, the plot was limited to a lateral radius of 20 mm from the beam axis. Beyond this radius, the dose contribution decreases sharply and remains negligible due to the limited lateral spread of the beam, which is mainly caused by multiple scattering processes. Including regions beyond 20 mm would not provide meaningful information, as the dose levels fall below the therapeutic threshold and would introduce unnecessary visual noise into the plot. This limitation is particularly justified in the case of superficial tumor treatments, such as ocular tumors (e.g., uveal melanoma), where the target volume lies at shallow depths and within a confined anatomical region.

This trend confirms that low-energy proton beams concentrate their dose within a narrower area, primarily because they exhibit significantly higher stopping power (dE/dx). As they travel through matter, low-energy protons decelerate rapidly, resulting in enhanced energy deposition across the entire volume they traverse, even near the surface. In contrast, high-energy protons interact less frequently and release their energy more gradually over a longer range, producing a broader but less intense dose distribution.

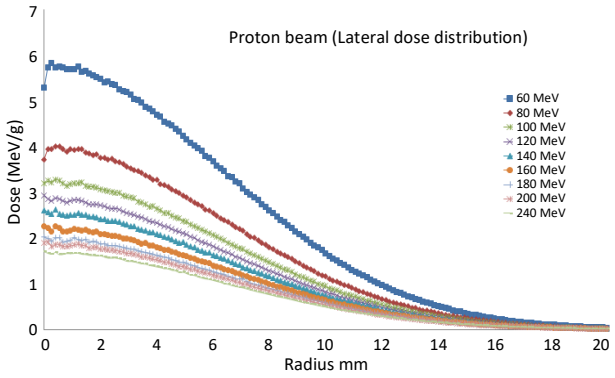

Fig. 1. Lateral dose distribution of a proton beam using energy from 60 to 240 MeV in 20 MeV increments.

Notably, Fig. 2 shows that 60 MeV protons deliver the highest integrated dose within the 20 mm lateral region, both at shallow and moderate depths. Although high-energy beams carry more total energy, the localized energy loss of low-energy protons leads to a greater dose concentration. This behavior is particularly advantageous for treating shallow tumors, where precise and confined irradiation is desired. In hadron therapy, this principle underpins the selection of beam energy according to tumor depth: lower energies for superficial lesions and higher energies for deeper-seated targets, thereby maximizing therapeutic impact while minimizing damage to surrounding healthy tissues.

For a helium-4 ion beams, the dose distributions are given in Fig. 2, which show that the maximum dose was reached at 200 MeV, with a value of 32.5 MeV/g at a radial position of 0.6 mm. For energies below 200 MeV, the deposited dose wasrelatively low, with 5.5E-2 MeV/g at 120 MeV and 10.9 MeV/g at 160 MeV. Conversely, beyond 200 MeV, the dose gradually decreased, recording 22.6 MeV/g at 240 MeV, 18.7 MeV/g at 280 MeV, 15.8 MeV/g at 320 MeV, 14.5 MeV/g at 360 MeV, 12.5 MeV/g at 400 MeV, 11.9 MeV/g at 440 MeV, 11.1 MeV/g at 480 MeV, and finally 10.1 MeV/g at 520 MeV. This gradual decline indicates that while high energies allow for greater penetration, they also lead to broader dose dispersion, reducing the energy concentration at a specific point. On the other hand, low-energy beams (≤200 MeV) interact strongly with the medium, resulting in rapid energy loss and a more localized dose deposition. At 200 MeV, the dose hit its peak and well confined, enabling precise targeting of a specific region with high impact. In contrast, at high energies (>200 MeV), the dose spreads out as particles travel deeper before being fully absorbed. This can be useful for treating larger tumor volumes but results in a lower energy concentration at any given point.

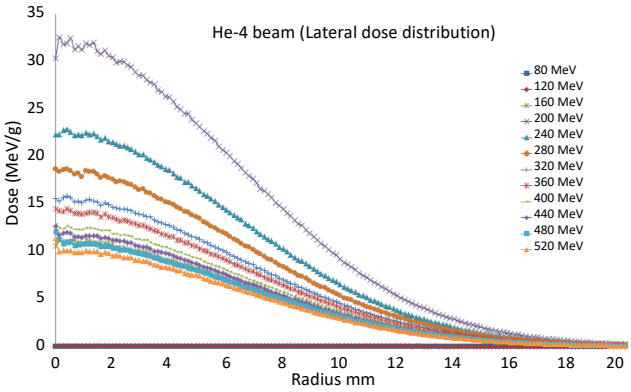

Fig. 2. Lateral dose distribution of a helium-4 ion beams using energy from 80 to 520 MeV in 40 MeV increments.

These observations are crucial for hadron therapy and heavy-ion radiotherapy, as they help optimize dose distribution according to therapeutic needs. In conclusion, 200 MeV appears to be the optimal energy for maximum dose concentration, while higher energies lead to progressive dispersion, emphasizing the importance of energy selection in medical treatment planning. By comparing Figs. 1 and 2, one can see that the lateral dose is higher in intensity for helium-4 ion beams compared to proton beams, at identical energies, which is expected because of the greater mass of helium-4 ions.

Depth dose distribution

Figure 3 illustrates the dose distribution as a function of depth in water for proton beams with energies ranging from 60 to 200 MeV. The observed behavior is characteristic of the interaction of charged particles with matter, including the presence of distinct Bragg peaks for each beam energy. Initially, the dose deposited was low in the early layers of the medium, followed by a rapid increase in energy deposition as the end of the particle's range which depends on the initial energy of the beam.

The dose distribution as a function of depth in water for a helium-4 ion beam is shown in Fig. 4. The behavior is similar to that of proton beams; however, at lower energies, the Bragg peaks are narrower and more intense, indicating a higher concentration of dose at a specific depth. For higher energies (above 400 MeV), the peaks become slightly broader due to scattering and secondary interactions of the particles within the medium. It is also noticeable that, for the same position of maximum energy deposition, helium-4 ion beams require significantly higher energies than proton beams. This is due to the higher mass and charge of helium-4 nuclei compared to protons, which leads to faster deceleration and more intense interactions with the medium.

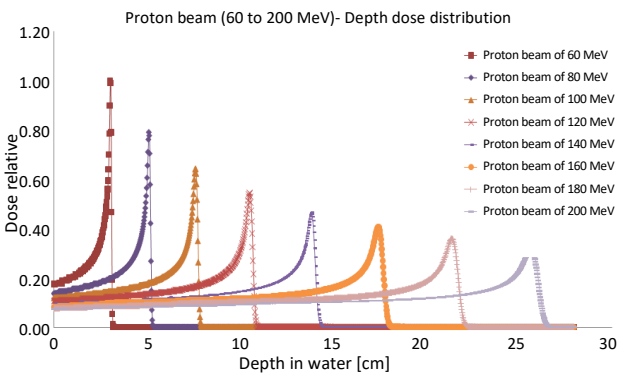

Fig. 3. Depth dose distribution in water for proton beams with energies ranging from 60 to 200 MeV in 20 MeV increments.

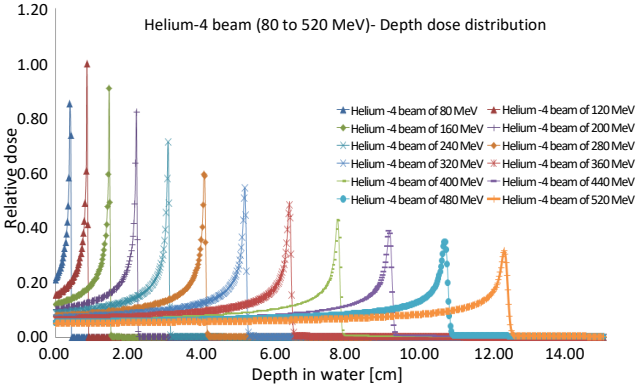

Fig. 4. Depth dose distribution in water for helium-4 ion beams with energies ranging from 80 to 520 MeV in 40 MeV increments.

Secondary particle dose calculations

The relative variation Δ, defined with (Eq.1).

$$\Delta = \left(\frac{Value\ (Helium{-}4) - Value\ (Proton)}{Value\ (Proton)} \right) \quad (1)$$

for each physical quantity was calculated by integrating the values for both proton and helium-4 ion beams. The results, presented in the Table 2, indicate that the use of helium-4 ion beams ledto a significant reduction in the dose deposited by neutrons and photons, reachedup to 82.56 %. This suggests that helium-4 ion beams generate less secondary radiation, offering a notable advantage in minimizing unwanted exposure to healthy tissues in hadron therapy.

In particular, proton fluence decreased drastically by 99.68 %, indicating a much lower production of secondary protons. Similarly, electron fluence dropped by 84.05 %, reducing contributions to low-energy radiation. Neutron and photon fluences also showed substantial reductions, ranging from 71 % to 82 %, highlighting decreased fragmentation and secondary interactions compared to protons.

Conversely, the production of heavy particles such as helium-3, helium ions, and other heavy ions increased significantly with helium-4 ion beams. Notably, helium ion fluence increased by 133,698 %, while helium-3 fluence rose by 16,855 %, reflecting a much higher nuclear fragmentation rate. This effect is crucial in hadron therapy, as helium-4 ions produce denser track structures, enhancing biological effectiveness in tumor destruction. However, this also necessitates precise control to limit collateral damage to healthy tissue.

Overall, the total number of detected photons and electrons decreased by 76.08 %, confirming that helium-4 ion interactions result in less secondary radiation. These results were obtained within a cylindrical volume measuring 0.40 mm in height and 0.15 mm in radius, defining the region where dose and fluence were analyzed.

CONCLUSION

This study used MCNP 6.3 to compare proton and helium-4 ion beams in terms of lateral dose, depth dose, and secondary particle production. Lateral dose analysis showed that helium-4 beams deliver higher peak doses than protons, with maximum concentration at 200 MeV. Depth dose profiles confirmed the presence of Bragg peaks for both beams; helium-4 ions required higher energies to reach the same depths due to their greater mass and charge. Secondary particle analysis revealed that helium-4 beams produce significantly fewer neutrons, photons, electrons, and secondary protons, while generating more heavy fragments such as helium-3 and other ions. These differences reflect the distinct interaction mechanisms of each beam type.

Table 2. Comparison of dose deposition of secondary particles for proton and helium-4 ion beams across different particle types.

Measurement type	Particle	Proton (Value ± Error)	Helium-4 ion (Value ± Error)	Unit	Relative variation (%)
Deposited Dose (Energy per Mass)	Neutron	2.01501E-05 ± 0.0010	6.24382E-06 ± 0.0022	MeV/g	69
Fluence (Number of Particles per Area)	Neutron	1.44953E-04 ± 0.0008	4.18180E-05 ± 0.0020	1/cm²	71.14
Deposited Dose (Energy per Mass)	Photon	9.76933E-05 ± 0.0010	1.70328E-05 ± 0.0039	MeV/g	82.56
Deposited Dose (Energy per Mass)	Photon	7.13265E-07 ± 0.0017	1.44453E-07 ± 0.0039	MeV/g	79.74
Total Detected Photons and Electrons	Photon/Electron	9.65435E-02 ± 0.0010	2.30837E-02 ± 0.0021	Count	76.08
Fluence (Number of Particles per Area)	Electron	3.12185E-06 ± 0.0017	4.98127E-07 ± 0.0043	1/cm²	84.05
Fluence (Number of Particles per Area)	Proton	8.36526E-04 ± 0.0001	2.63467E-06 ± 0.0022	1/cm²	99.68
Fluence (Number of Particles per Area)	Deuteron	1.38304E-06 ± 0.0029	1.20320E-06 ± 0.0034	1/cm²	13
Fluence (Number of Particles per Area)	Helium-3	2.44160E-09 ± 0.0085	4.13907E-07 ± 0.0028	1/cm²	16855.1
Fluence (Number of Particles per Area)	Helium	5.69438E-08 ± 0.0023	7.61523E-05 ± 0.0001	1/cm²	133698.9
Fluence (Number of Particles per Area)	Heavy Ion	1.26888E-09 ± 0.0032	2.73811E-09 ± 0.0024	1/cm²	115.88

ACKNOWLEDGMENT

The authors gratefully acknowledge their respective institutions for providing the facilities and support necessary to carry out this research. They also thank all colleagues who contributed through valuable discussions and technical assistance during the course of this work.

AUTHOR CONTRIBUTION

O. Allaoui: Conceptualization, methodology, writing original draft preparation. A. Didi: Conceptualization, supervision, methodology, validation, formal analysis, interpretation of results, writing review and editing, project administration. E. M. Alibrahmi: Supervision, conceptualization, methodology, validation, scientific guidance, writing review and editing. E. M. Chakir: Supervision, Z. Sadoune: scientific guidance.

REFERENCES

1. W. A. G. Sauerwein, K. Igawa, J. Herault *et al.,* Health Technol. **14** (2024) 995.
2. B. T. Essakpa, R. Sebihi, A. Didi *et al.,* Ann. Univ. Craiova Phys. **32** (2022) 9.
3. A. Didi, H. Dekhissi, Y. Mohamed *et al.,* Ann. Univ. Craiova Phys. **29** (2019) 77.
4. M. Yjjou, H. Dekhissi, J. Derkaoui *et al.,* Moscow Univ. Phys. Bull. **76** (2021) S8.
5. S. Lorenzoni, C. Rodríguez-Nogales, M. J. Blanco-Prieto *et al.,* Cancer Lett. **614** (2025) 217536.
6. O. M. Kutova, E. L. Guryev, E. A. Sokolova *et al.,* Cancer **11** (2029) 1.
7. U. Amaldi, Health Technol. **14** (2024) 823.
8. X. H. Zhu, J. X. Du, D. Zhu *et al.,* Oxid. Med. Cell. Longevity **18** (2020) 5721258.
9. M. Jiang, B. Qin, L. Luo *et al.,* J. Controlled Release **335** (2021) 408.
10. S. M. Valle, Helium Ion Beams for Eye Treatment: an in Silico Investigation, Master's Thesis, Università Degli Studi di Pavia, Pavia (2014).
11. A. Didi, H. Dekhissi, R. Sebihi *et al.* Moscow Univ. Phys. Bull. **74** (2019) 364.
12. L. Volz, C. A. Collins-Fekete, E. Bär *et al.,* Phys. Med. Biol. **66** (2021) 23501.
13. J. S. Bull, MCNP6.2 and MCNP6.3 Performance Comparison, Los Alamos National Laboratory Presentation LA-UR-23-30469, Rev. 1., New Mexico, United States (2023).
14. R. Juarez, M. Belotti, A. Kolsek *et al.,* Nat. Commun. **15** (2024) 8563.
15. E. Asano, D. Coleman, G. Davidson *et al.,* Nucl. Instrum. Methods Phys. Res., Sect. A **1031** (2022) 166568.
16. M. J. Berger, J. S. Coursey, M. A. Zucker *et al.,* Stopping-Power & Range Tables for Electrons, Protons, and Helium Ions, NIST Standard Reference Database 124. https://www.nist.gov/pml/stopping-power-range-tables-electrons-protons-and-helium-ions. Retrieved in February (2025)
17. J. Liu, S. Yan, J. Xue *et al.,* Nucl. Instrum. Methods Phys. Res., Sect. B **478** (2020) 187.
18. T. E. Bakolia, A. Didi, R. Sebihi *et al.,* Atom Indones. **50** (2024) 37.
19. H. El Bekkouri, E. Al Ibrahmi, M. El-Asery *et al.,* Atom Indones. **50** (2024) 135.
20. M. El-Asery, Z. Sadoune, H. El Bekkouri *et al.,* Moscow Univ. Phys. Bull. **78** (2023) 810.
21. E. M. Essaidi, M. Krim, O. Kaanouch *et al.,* Atom Indones. **51** (2025) 109.
22. A. Sari, F. Carrel, F. Lainé, IEEE Trans. Nucl. Sci. **65** (2018) 2539.
23. International Commission on Radiation Units & Measurements, ICRU Report 78, Prescribing, Recording, and Reporting Proton-Beam Therapy. https://www.icru.org/report/prescribing-recording-and-reporting-proton-beam-therapy-icru-report-78/. Retrieved in February (2025)
24. S. Mao, K. Xiao, W. Zhou *et al.,* J. Pain Res. **16** (2023) 3925.
25. A. C. Kraan, Front. Oncol. **5** (2015) 150.